Anatomy of Spin-Transfer Torque

M.D. Stiles

National Institute of Standards and Technology, Gaithersburg, MD 20899-8412

A. Zangwill

School of Physics, Georgia Institute of Technology, Atlanta, GA 30332-0430

(Dated: May 8, 2002)

Spin-transfer torques occur in magnetic heterostructures because the transverse component of a spin current that flows from a non-magnet into a ferromagnet is absorbed at the interface. We demonstrate this fact explicitly using free electron models and first principles electronic structure calculations for real material interfaces. Three distinct processes contribute to the absorption: (1) spin-dependent reflection and transmission; (2) rotation of reflected and transmitted spins; and (3) spatial precession of spins in the ferromagnet. When summed over all Fermi surface electrons, these processes reduce the transverse component of the transmitted and reflected spin currents to nearly zero for most systems of interest. Therefore, to a good approximation, the torque on the magnetization is proportional to the transverse piece of the incoming spin current.

I. INTRODUCTION

When a current of polarized electrons enters a ferromagnet, there is generally a transfer of angular momentum between the propagating electrons and the magnetization of the film. This concept of "spin transfer" was proposed independently by Slonczewski[1] and Berger[2] in 1996. Experiments soon followed where anomalies in the current-voltage characteristics of magnetic heterostructures were interpreted as evidence for spin transfer.[3] Unambiguous confirmation came when the phenomenon of giant magnetoresistance[4] was used to detect magnetization reversal in ferromagnetic multilayers with large current densities flowing perpendicular to the plane of the layers.[5–7] Subsequently, spin transfer has been implicated to explain the observation of spin precession for high-energy, spin-polarized electrons that traverse a magnetic thin film[8] and enhanced Gilbert damping in magnetic multilayers compared to one-component magnetic films.[9] More experiments may be expected in the future because spin transfer is expected to play an important role in the nascent field of "spin electronics".[10]

Theoretical work on spin transfer generally falls into one of three categories. One group of articles focuses on deriving and solving classical equations of motion for the magnetization.[11–16] These studies generalize the Landau-Lifshitz equation to take account of spin currents, spin accumulation,[17] and the mechanical torques which necessarily accompany (spin) angular momentum transfer. A second group of articles generalizes charge transport theory to take account of spin currents and spin relaxation.[18–22] These theories compute the spin-transfer torques that serve as input to the magnetization calculations. The torque can be computed phenomenologically, or from the Boltzmann, Kubo or Landauer formalisms that incorporate quantum mechanical information explicitly. Finally, there are articles that report quantum mechanical calculations of the parameters that serve as input to the transport theories. The model studies of Slonczewski[1] and Berger[2] are of this sort, as are the first-principles, electronic structure calculations of Xia and co-workers.[23]

In a previous paper,[22] the present authors used a 2×2 matrix Boltzmann equation to compute spin currents, spin accumulation, magnetoresistance, and spin-transfer torques in a Co/Cu/Co multilayer with non-collinear magnetization. The physics of spin transfer entered this semi-classical, kinetic theory calculation through quantum mechanically derived matching conditions imposed at each ferromagnet/non-magnet interface. Specifically, we took account of a *reflection mechanism*[1] that arises because the interface reflection and transmission amplitudes for polarized electrons are spin dependent. We also took account of an *averaging mechanism*[2] that arises because conduction electron spins precess around the magnetization vector in each ferromagnet. The present work was motivated originally by two assumptions we made to simplify the Co/Cu/Co calculations. First, we set to zero the transverse component of the spin of the conduction electron ensemble in each ferromagnet. Second, we disregarded the phase of the reflection and transmission amplitudes. As best we can determine, the same assumptions are implicit in the Landauer-type model calculations reported in Ref. 19 and Ref. 20. Therefore, before calculations of this sort are carried very much further, it seemed appropriate to look more carefully into the correctness of these assumptions. As we will see the spin transfer process is more subtle and complex than previously managed.

In this paper, we analyze quantum mechanically the fate of a polarized current that enters a ferromagnet from a metallic non-magnet. Using both the free electron model and first principles electronic structure calculations, we conclude that the assumptions in question are largely justified. An important point is that the spin of an electron generally rotates when it is reflected or transmitted at an interface. This separates the reflection mechanism into two pieces. A spin-filter effect reduces the transverse spin component of each electron individually. A further reduction occurs when we sum over all

Fermi surface electrons because substantial phase cancellation occurs when the distribution of spin rotation angles is broad. As for the mechanism we called "averaging" in Ref. 22, cancellation occurs because electrons have different precession frequencies.[24] This leads to an asymptotic, oscillatory, power-law (rather than exponential) decay of the transmitted transverse spin component. Putting everything together, we find that (except in very exceptional cases) the transverse spin current is almost completely absorbed within a few lattice constants of the interface. None, or very little, is reflected or transmitted. As a result, the spin-transfer torque is very nearly proportional to the transverse piece of the incident spin current.

The plan of this paper is as follows. In Section II, we define the basic variables of spin transport and establish our notation. Section III analyzes the spin current and spin-transfer torque near a magnetic/non-magnetic interface using a free electron model for both materials. Section IV generalizes the analysis of Section III to the case of real materials. We summarize our results in Section V.

II. BACKGROUND

To help introduce the theory of spin transport, it is useful first to set down the familiar equations of particle transport. These involve the number density,

$$n(\mathbf{r}) = \sum_{i\sigma} \psi_{i\sigma}^*(\mathbf{r})\,\psi_{i\sigma}(\mathbf{r}), \qquad (1)$$

and the number current density,

$$\mathbf{j}(\mathbf{r}) = \mathrm{Re}\sum_{i\sigma} \psi_{i\sigma}^*(\mathbf{r})\,\hat{\mathbf{v}}\,\psi_{i\sigma}(\mathbf{r}), \qquad (2)$$

where $\hat{\mathbf{v}} = -(i\hbar/m)\nabla$ is the velocity operator and $\psi_{i,\sigma}(\mathbf{r})$ is an occupied single particle wave function with state index i and spin index σ. The continuity equation,

$$\nabla \cdot \mathbf{j} + \frac{\partial n}{\partial t} = 0, \qquad (3)$$

expresses the conservation of particle number. In this paper, we will be interested exclusively in steady-state situations where the time derivative in (3) is zero. Not far from equilibrium, the current takes the phenomenological form,

$$\mathbf{j} = (\sigma/e)\mathbf{E} - D\nabla\delta n, \qquad (4)$$

where $\delta n = n - n_{\mathrm{eq}}$ is the deviation of the number density from its equilibrium value, $\mathbf{E}$ is an electric field, σ is the conductivity, and D is a diffusion constant. The latter two are second rank tensors in the general case.

For the spin degree of freedom, the analogs to (1) and (2) are the spin density,

$$\mathbf{m}(\mathbf{r}) = \sum_{i\sigma\sigma'} \psi_{i\sigma}^*(\mathbf{r})\,\mathbf{s}_{\sigma,\sigma'}\,\psi_{i\sigma'}(\mathbf{r}), \qquad (5)$$

and the spin current density

$$\mathbf{Q}(\mathbf{r}) = \sum_{i\sigma\sigma'} \mathrm{Re}\left[\psi_{i\sigma}^*(\mathbf{r})\,\mathbf{s}_{\sigma,\sigma'}\otimes\hat{\mathbf{v}}\,\psi_{i\sigma'}(\mathbf{r})\right], \qquad (6)$$

where $\mathbf{s} = (\hbar/2)\boldsymbol{\sigma}$ and $\boldsymbol{\sigma}$ is a vector whose Cartesian components are the three Pauli matrices. The spin current is a tensor quantity. The left index of $Q_{ij}(\mathbf{r})$ is in spin space and the right index is in real space. Spin is not conserved so the analog of (3) generally has non-zero terms on the right hand side. For our problem,

$$\nabla \cdot \mathbf{Q} + \frac{\partial \mathbf{m}}{\partial t} = -\frac{\delta\mathbf{m}}{\tau_{\uparrow\downarrow}} + \mathbf{n}_{\mathrm{ext}} \qquad (7)$$

where $\mathbf{n}_{\mathrm{ext}}$ is an external torque density, $\nabla \cdot \mathbf{Q} = \partial_k Q_{ik}$ and $\delta\mathbf{m} = (|\mathbf{m}| - m_{\mathrm{eq}})\hat{\mathbf{m}}$ is the so-called *spin accumulation*.[17] The first term on the right side of (7) accounts for the transfer of angular momentum between the spin current and the lattice due to spin-flip. This process, with relaxation time $\tau_{\uparrow\downarrow}$, changes the magnitude of the local spin density, but not its direction. The second term on the right side of (7) describes all external torques that act to change the direction of the local magnetization. For example, the Landau-Lifshitz-Gilbert torque density,

$$\mathbf{n}_{\mathrm{ext}} = -(g\mu_{\mathrm{B}}/\hbar)\mathbf{m}\times\mathbf{B}_{\mathrm{eff}} + \alpha\,\hat{\mathbf{m}}\times\dot{\mathbf{m}} \qquad (8)$$

includes an effective field $\mathbf{B}_{\mathrm{eff}}$ and phenomenological damping. The effective field is due to exchange, anisotropies, and any external fields that might be present.

To study magnetization dynamics, we merely rearrange (7) to

$$\frac{\partial \mathbf{m}}{\partial t} = \mathbf{n}_{\mathrm{c}} + \mathbf{n}_{\mathrm{ext}} \qquad (9)$$

where

$$\mathbf{n}_{\mathrm{c}} = -\frac{\delta\mathbf{m}}{\tau_{\uparrow\downarrow}} - \nabla \cdot \mathbf{Q} \qquad (10)$$

is the current-induced contribution to the torque density. The divergence theorem then shows that, apart from spin-flip, the torque on the total magnetization in a volume V arises from the net flux of spin current into and out of the surface S that bounds V. Phenomenologically, the spin current is driven by drift and diffusion:

$$Q_{ik} = \bar{\sigma}_i E_k - \bar{\Lambda}_i \partial_k \delta n - \bar{D}\partial_k \delta m_i \qquad (11)$$

As in (4), we assume the simplest form for the spin transport coefficients. That is, we use the vectors $\bar{\boldsymbol{\sigma}} = (\sigma_\uparrow - \sigma_\downarrow)\hat{\mathbf{m}}$ and $\bar{\boldsymbol{\Lambda}}$ (also proportional to $\sigma_\uparrow - \sigma_\downarrow$) rather than third rank tensors and the scalar $\bar{D}$ rather than a fourth rank tensor. The conductivities $\sigma_\uparrow$ and $\sigma_\downarrow$ refer to majority and minority electrons, respectively.

In a non-magnet, $\sigma_\uparrow = \sigma_\downarrow$ and the first two terms on the right side of (11) are zero. A spin current arises

only if there are regions of the metal where there is a gradient in the spin accumulation, $\delta\mathbf{m}(\mathbf{r})$. This implies that the spin density $\mathbf{m}(\mathbf{r})$ and the spin current density $\mathbf{Q}(\mathbf{r})$ are only indirectly related to each other. For example, the projection of spin current along the current $\mathbf{Q}(\mathbf{r})\cdot\mathbf{j}(\mathbf{r})$, a vector proportional to the "polarization" of the current, need not be collinear with the spin accumulation $\delta\mathbf{m}(\mathbf{r})$. In a ferromagnet, an electric field and/or a number density gradient produce a current of polarized spins simply because $\sigma_\uparrow \neq \sigma_\downarrow$. This spin current is modified by gradients in spin accumulation also. However, the transport equations (4) and (11) are valid (at most) when the direction of the ferromagnetic magnetization is uniform in space. Corrections are necessary when the magnetization rotates continuously in space, *e.g.*, inside a domain wall.[11] Finally, a comparison of (11) with (4) suggests that gradients in spin accumulation ought to induce a conventional particle current as well. We account for this possibility by amending (4) to read

$$j_i = (\sigma/e)E_i - D\partial_i\delta n - \Lambda_k\partial_i\delta m_k. \qquad (12)$$

With this background, the remainder of this paper is devoted to a detailed analysis of the fate of a spin polarized current that flows from a metallic non-magnet into a metallic, single-domain ferromagnet through an ideal, flat interface. Specifically, we point the particle current density vector $\mathbf{j}$ along positive $\hat{\mathbf{x}}$, we point the ferromagnetic magnetization vector $\mathbf{M}$ along positive $\hat{\mathbf{z}}$, and we fix the interface at $x = 0$. Figure 1 shows three possible steady states of pure current polarization in the non-magnet and the associated non-zero component of the spin current density tensor. For each case, we let only one component of $Q_{\alpha x}$ be non-zero. $Q_{zx} \neq 0$ corresponds to longitudinal (parallel to $\mathbf{M}$) current polarization. $Q_{xx} \neq 0$ or $Q_{yx} \neq 0$ correspond to transverse (perpendicular to $\mathbf{M}$) current polarization. To produce an "incident" polarized current in the non-magnet, it is sufficient that the current flow into the non-magnet from an adjacent ferromagnet and that the thickness of the non-magnet be small compared to the non-magnet spin-flip diffusion length.[17] For this reason, magnetic multilayer structures are the rule in most spin-transfer experiments. We refer the reader to Ref. 22 for some insight into the polarization process for the Co/Cu/Co system.

Figure 1 also indicates that, of the three incident states of pure current polarization shown, only Q_{zx} transmits into the bulk of the ferromagnet. The magnet absorbs the transverse components. Furthermore (see below), almost none of the transverse spin current reflects from the interface. Therefore, if we choose a rectangular pillbox that just straddles the interface, the divergence theorem discussion below (10) implies that a current-induced spin-transfer torque is exerted on the interfacial magnetization. To be more precise, Figure 2 illustrates such a pillbox and incident, reflected, and transmitted charge current density vectors. Integrating the steady state ($\dot{\rho} = 0$) version of the continuity equation (3) over the pillbox
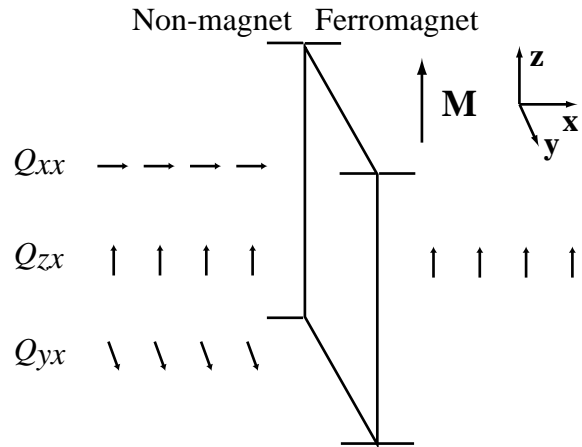

FIG. 1: Three states of spin current scatter from an interface. The current flows from left-to-right, from the non-magnet into the ferromagnet. Q_{zx} is longitudinal (parallel) to the magnetization $\mathbf{M}$. Q_{xx} and Q_{yx} are transverse to $\mathbf{M}$. Only Q_{zx} can be non-zero in the bulk of the magnet. The transverse spin currents are absorbed in the interfacial region.

gives

$$0 = (\mathbf{j}^{\text{in}} - \mathbf{j}^{\text{tr}} + \mathbf{j}^{\text{ref}}) \cdot A\hat{\mathbf{x}} \qquad (13)$$

where A is the area of the interface. Eq. (13) says that the incoming flux $\mathbf{j}^{\text{in}} \cdot A\hat{\mathbf{x}}$ minus the outgoing flux $\mathbf{j}^{\text{tr}} \cdot A\hat{\mathbf{x}} + \mathbf{j}^{\text{ref}} \cdot (-A\hat{\mathbf{x}})$ equals zero. The reflected flux has a minus sign relative to the transmitted flux because it passes through the opposing face of the pillbox.

Ignoring spin flip, the same integration applied to (10) yields

$$\mathbf{N}_c = (\mathbf{Q}^{\text{in}} - \mathbf{Q}^{\text{tr}} + \mathbf{Q}^{\text{ref}}) \cdot A\hat{\mathbf{x}} \simeq \mathbf{Q}^{\text{in}}_\perp \cdot A\hat{\mathbf{x}} \qquad (14)$$

where $\mathbf{Q}^{\text{in}}$, $\mathbf{Q}^{\text{ref}}$, and $\mathbf{Q}^{\text{tr}}$ are the spin current density (6) computed using incident state, reflected state, and transmitted state wave functions. Eq. (14) says that the incoming spin flux $\mathbf{Q}^{\text{in}} \cdot A\hat{\mathbf{x}}$ minus the outgoing spin flux $\mathbf{Q}^{\text{tr}} \cdot A\hat{\mathbf{x}} + \mathbf{Q}^{\text{ref}} \cdot (-A\hat{\mathbf{x}})$ equals the torque on the magnetization inside the pillbox.[25] The torque $\mathbf{N}_c$ is a vector in spin space because we have contracted the space index of the spin current density with the space vector $\hat{\mathbf{x}}$. The approximate form on the right of Eq. (14) says that the torque is proportional to the transverse part of $\mathbf{Q}_{\text{in}}$. That is the main message of this paper. The following sections are devoted to a demonstration that the transverse transmitted and reflected spin currents do indeed disappear in the immediate vicinity of the interface.

III. FREE ELECTRONS

In this section, we compute the spin current near the interface of a non-magnet and a ferromagnet assuming that a free electron description is adequate for the conduction electrons in the non-magnet and also for both
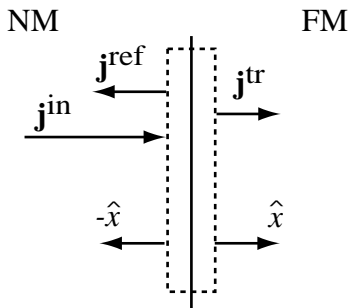
FIG. 2: Interfacial pillbox used as the integration volume when the divergence theorem is applied to (3) and (10) to derive (13) and (14).

the majority and minority conduction electrons in the ferromagnet. We do this in the interest of analytic simplicity and also because some authors[13,15] believe this is a fair representation of reality for the purposes of transport calculations.

We first work out the problem of one electron scattering from a planar interface to determine the amplitudes for reflection and transmission. They turn out to be spin dependent. As first shown by Slonczewski,[1] this fact alone generates a "spin-filter" torque because the wave function for an incident electron with a non-zero component of spin transverse to $\mathbf{M}$ can always be re-expressed in terms of up and down spin components.

The actual current polarization in the metal is obtained by summing over the full distribution of conduction electrons. This introduces two effects. The first arises because the reflection amplitude for free electron interface scattering is complex. This means that the spin of an incoming electron rotates upon reflection. The cancellation which occurs when we sum over all these spin vectors reduces the net transverse spin current because reflection and transmission both contribute to the outgoing flux from the interface region. A second effect arises because up and down spin electrons on the Fermi surface with the same wave vector in the non-magnet no longer have the same wave vector when they transmit into the ferromagnet. The two states are coherent, so precession in space (rather than time) occurs. The precession frequency is different for electrons from different portions of the Fermi surface. Therefore, when we sum over all conduction electrons, almost complete cancellation of the transverse spin occurs after propagation into the ferromagnet by a few lattice constants.

A. Spin currents for a single electron

Let us choose the spin quantization axis to be parallel to the magnetization of the ferromagnet. Then, in the non-magnet, the wave function for an electron whose spin points in an arbitrary direction can always be written as a linear combination of spin up and spin down components.

Specifically,

$$\psi_{\text{in}} = \left[\cos \tfrac{1}{2}\theta\, e^{-i\phi/2}\, |\!\uparrow\rangle + \sin \tfrac{1}{2}\theta\, e^{i\phi/2}\, |\!\downarrow\rangle\right] e^{ik_x x} e^{i\mathbf{q}\cdot\mathbf{R}} \quad (15)$$

represents a free electron propagating toward the interface in Figure 1 with its spin pointed in the direction (θ, ϕ) with respect to $\mathbf{M}$. We are interested in conduction electrons so the wave vector $\mathbf{k} = (k_x, \mathbf{q})$ satisfies $\hbar k^2/2m = E_{\text{F}}$. The spatial variable is $\mathbf{r} = (x, \mathbf{R})$. As the notation indicates, (15) is the incident state for a scattering problem that determines the wave function for the entire system. The latter describes a steady-state situation like current flow.[26] Like the incident state (15), the complete scattering state can also be written as a linear combination of spin up and spin down components:

$$\psi = \psi_\uparrow + \psi_\downarrow. \quad (16)$$

In detail,

$$\psi_\uparrow = \cos \tfrac{1}{2}\theta\, e^{-i\phi/2}\, |\!\uparrow\rangle \begin{cases} (e^{ik_x x} + R_\uparrow e^{-ik_x x})e^{i\mathbf{q}\cdot\mathbf{R}} & x < 0 \\ T_\uparrow e^{ik_x^\uparrow x} e^{i\mathbf{q}\cdot\mathbf{R}} & x > 0 \end{cases}$$

$$\psi_\downarrow = \sin \tfrac{1}{2}\theta\, e^{i\phi/2}\, |\!\downarrow\rangle \begin{cases} (e^{ik_x x} + R_\downarrow e^{-ik_x x})e^{i\mathbf{q}\cdot\mathbf{R}} & x < 0 \\ T_\downarrow e^{ik_x^\downarrow x} e^{i\mathbf{q}\cdot\mathbf{R}} & x > 0 \end{cases}$$

$$(17)$$

where $R_\uparrow$, $R_\downarrow$, $T_\uparrow$, and $T_\downarrow$ are the reflection and transmission amplitudes for up and down spin electrons. These amplitudes do not depend on the angles θ and ϕ. Notice that the up and down spin components do not propagate with the same wave vector for $x > 0$. The wave vectors differ because their kinetic energy depends on the exchange potential energy in the ferromagnet. The common factor of $\exp(i\mathbf{q}\cdot\mathbf{R})$ in (17) reminds us that scattering from a flat interface conserves the wave vector component parallel to the interface.

The transmission and reflection amplitudes are determined by the magnitude of the potential step at the interface. For a constant effective mass, this step height is parameterized by $k_{\text{F}}, k_{\text{F}}^\uparrow$, and $k_{\text{F}}^\downarrow < k_{\text{F}}^\uparrow$, the Fermi wave vectors for, respectively, electrons in the non-magnet, majority electrons in the ferromagnet, and minority electrons in the ferromagnet. The usual quantum mechanical matching conditions yield the *real* transmission amplitudes

$$T_\sigma(q) = \frac{2k_x(q)}{k_x(q) + k_x^\sigma(q)} \quad (18)$$

where $k_x(q) = \sqrt{k_{\text{F}}^2 - q^2}$ and $k_x^\sigma(q) = \sqrt{(k_{\text{F}}^\sigma)^2 - q^2}$. The reflection amplitudes are real or complex depending on the magnitude of the parallel wave vector. They are

$$R_\sigma(q) = \frac{k_x(q) - k_x^\sigma(q)}{k_x(q) + k_x^\sigma(q)} \qquad \text{if} \qquad q^2 \leq (k_{\text{F}}^\sigma)^2 \quad (19)$$

and

$$R_\sigma(q) = \frac{k_x(q) - i\kappa_x^\sigma(q)}{k_x(q) + i\kappa_x^\sigma(q)} \qquad \text{if} \qquad q^2 > (k_{\text{F}}^\sigma)^2 \quad (20)$$

where $\kappa_x^\sigma(q) = \sqrt{q^2 - k_F^{\sigma\,2}}$. The associated transmission and reflection *probabilities*,

$$
\begin{aligned}
\mathrm{R}^\sigma(q) &= |R_\sigma(q)|^2 \\
\mathrm{T}^\sigma(q) &= \frac{k_x^\sigma(q)}{k_x(q)}|T_\sigma(q)|^2,
\end{aligned}
\tag{21}
$$

satisfy $\mathrm{R}^\sigma + \mathrm{T}^\sigma = 1$ and are plotted in Figure 3 for a slice through the free electron Fermi surfaces defined by $k_F^\uparrow/k_F = 1.5$ and $k_F^\downarrow/k_F = 0.5$. For this case, the transmission probability for majority electrons (dashed curve) is unity near the zone center and then falls rapidly to zero near k_F. The minority electrons (solid curve) transmit similarly except that $\mathrm{T}^\downarrow$ falls to zero near $k_F^\downarrow$.

It is now straightforward to compute and interpret the incident, reflected, and transmitted number current densities and spin current densities. We need only (2), (6), and the appropriate piece of the wave function (17). The incident current densities are

$$
\begin{aligned}
j_x^{\mathrm{in}} &= v_x \\
Q_{xx}^{\mathrm{in}} &= \frac{\hbar}{2}v_x \sin\theta\cos\phi \\
Q_{yx}^{\mathrm{in}} &= \frac{\hbar}{2}v_x \sin\theta\sin\phi \\
Q_{zx}^{\mathrm{in}} &= \frac{\hbar}{2}v_x \cos\theta
\end{aligned}
\tag{22}
$$

where $v_x = \hbar k_x/m$. The reflected current densities are

$$
\begin{aligned}
j_x^{\mathrm{ref}} &= -|v_x|\left[\cos^2\tfrac{1}{2}\theta\,|R_\uparrow|^2 + \sin^2\tfrac{1}{2}\theta\,|R_\downarrow|^2\right] \\
Q_{zx}^{\mathrm{ref}} &= -\frac{\hbar}{2}|v_x|\left[\cos^2\tfrac{1}{2}\theta\,|R_\uparrow|^2 - \sin^2\tfrac{1}{2}\theta\,|R_\downarrow|^2\right] \\
Q_{xx}^{\mathrm{ref}} &= -\frac{\hbar}{4}|v_x|\sin\theta\,\mathrm{Re}\left[R_\uparrow^* R_\downarrow e^{-i\phi}\right] \\
Q_{yx}^{\mathrm{ref}} &= -\frac{\hbar}{4}|v_x|\sin\theta\,\mathrm{Im}\left[R_\uparrow^* R_\downarrow e^{-i\phi}\right].
\end{aligned}
\tag{23}
$$

The transmitted current densities are

$$
\begin{aligned}
j_x^{\mathrm{tr}} &= v_x^\uparrow \cos^2\tfrac{1}{2}\theta\,|T_\uparrow|^2 + v_x^\downarrow \sin^2\tfrac{1}{2}\theta\,|T_\downarrow|^2 \\
Q_{zx}^{\mathrm{tr}} &= \frac{\hbar}{2}v_x^\uparrow \cos^2\tfrac{1}{2}\theta\,|T_\uparrow|^2 - \frac{\hbar}{2}v_x^\downarrow \sin^2\tfrac{1}{2}\theta\,|T_\downarrow|^2 \\
Q_{xx}^{\mathrm{tr}}(\mathbf{r}) &= \frac{\hbar}{4}\frac{v_x^\uparrow + v_x^\downarrow}{2}\sin\theta\,\mathrm{Re}\left[T_\uparrow^* T_\downarrow e^{-i\phi}e^{i(k_x^\downarrow - k_x^\uparrow)x}\right] \\
Q_{yx}^{\mathrm{tr}}(\mathbf{r}) &= \frac{\hbar}{4}\frac{v_x^\uparrow + v_x^\downarrow}{2}\sin\theta\,\mathrm{Im}\left[T_\uparrow^* T_\downarrow e^{-i\phi}e^{i(k_x^\downarrow - k_x^\uparrow)x}\right]
\end{aligned}
\tag{24}
$$

where $v_x^\sigma = \hbar k_x^\sigma/m$. Using (21), it is easy to check that $j_x^{\mathrm{in}} = j_x^{\mathrm{tr}} - j_x^{\mathrm{ref}}$ and $Q_{zx}^{\mathrm{in}} = Q_{zx}^{\mathrm{tr}} - Q_{zx}^{\mathrm{ref}}$. The first relation is consistent with (13) because there is no accumulation of charge at the interface. Using (14), the second relation tells us that there is no torque associated with the transport of longitudinal spin current. However, a similar relationship does *not* hold for the other two components

of $\mathbf{Q}$. There is a discontinuity in the transverse spin current when a spin scatters from an interface. According to (14), this implies that a current-induced torque acts on the magnetization. In fact, three distinct mechanisms contribute to the net torque.

One source of discontinuity and spin-transfer torque is *spin filtering*. This occurs when the reflection probabilities are spin dependent.[1] To see this, note first that the specific superposition of up and down spin components displayed in the incident state wave function (15) corresponds to a specific transverse component of the spin vector. If $R_\uparrow = R_\downarrow$ and $T_\uparrow = T_\downarrow$, that specific linear combination is preserved in the reflected and transmitted pieces of the scattering state and no discontinuity occurs in the spin current. However, if the reflection and transmission amplitudes *differ* for up and down spin components, the up and down spin content of the spatially separated reflected and transmitted states differ from one another. This leads unavoidably to different transverse spin components and thus to a discontinuity in the transverse spin current. Given the structure of (23) and (24), we use the reflection and transmission *probabilities* in the combination $\sqrt{\mathrm{R}^\uparrow \mathrm{R}^\downarrow} + \sqrt{\mathrm{T}^\uparrow \mathrm{T}^\downarrow}$ as a measure of the ability of spin filtering to provide spin-transfer torque. The next-to-top and next-to-bottom panels in Figure 3 display the required information.

A second source of transverse spin current discontinuity and spin-transfer torque is *spin rotation*. This occurs when the product $R_\uparrow^* R_\downarrow$ is not positive real. Specifically, (23) shows that the transverse components of the reflected spin current contain a factor

$$
R_\uparrow^* R_\downarrow = |R_\uparrow^* R_\downarrow|e^{i\Delta\phi}.
\tag{25}
$$

The phase $\Delta\phi$ evidently adds directly to the azimuthal angle ϕ used to define the spin direction in the incident state vector (15). In other words, the reflected spin direction rotates with respect to the incident spin direction. This is an entirely quantum mechanical phenomenon for which there is no classical analog. The bottom panel of Figure 3 shows that the range of $\Delta\phi$ can be surprisingly large. Indeed, for this choice of Fermi surfaces, the spin direction completely reverses when an electron reflects from the interface at near-normal incidence. There is no corresponding rotation for transmitted electrons because $T_\uparrow$ and $T_\downarrow$ are positive real (for free electrons). The resulting discontinuity in the transverse spin current leads to a spin-transfer torque that is distinct from spin filtering.

Finally, a glance at (24) reveals that *spin precession* is a third source of spin-transfer torque. Note specially the spatially-varying phase factors which appear in the transmitted transverse spin currents because $k_x^\uparrow \neq k_x^\downarrow$ in the ferromagnet. Their net effect is spatial precession because Q_{xx} and Q_{yx} simply rotate into one another as a function of x.[27] From (10), such a spatial variation of $\mathbf{Q}$ contributes a distributed torque density at every point in the ferromagnet. The top panel of Figure 3 shows the
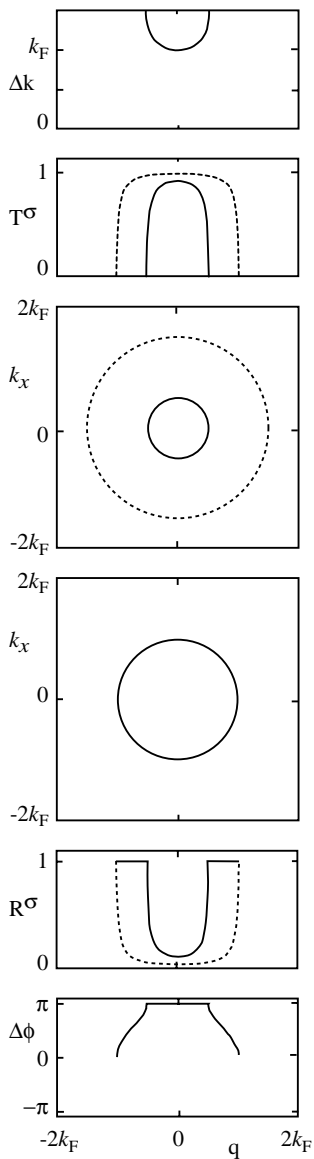
FIG. 3: Slices through a set of free electron Fermi surfaces. The two middle panels show the Fermi surface for the non-magnet and the superimposed Fermi surfaces of the majority (dashed) and minority (solid) states of the ferromagnet. The panel just above the magnetic Fermi surfaces is the probability for transmission into the ferromagnet for majority (dashed) and minority (solid) electrons. The panel just below the non-magnetic Fermi surface is the probability for reflection back into the non-magnet for majority (dashed) and minority (solid) electrons. The bottom panel shows the phase in (25) acquired by an electron because its spin rotates upon reflection. The top panel shows the wave vector difference (26) for a transmitted electron.

range of spatial precession "frequencies"

$$\Delta\mathrm{k} = k_x^{\downarrow} - k_x^{\uparrow} \quad (26)$$

for the free electron model of that figure.

B. Spin currents for a distribution of electrons

The spin currents relevant to experiment reflect the combined effect of all the conduction electrons. In the most general description of transport, it is necessary to keep track of the quantum mechanical coherence between all electrons in different eigenstates. However, to model the spin-transfer torque experiments reported to date,[5,6] it is not necessary to maintain the coherence between states with different Fermi surface wave vectors. It is sufficient to use a semi-classical theory that maintains only the coherence between up and down spin states at each $\mathbf{k}$-point on the Fermi surface. Accordingly, we define a 2×2 electron occupancy distribution matrix

$$\mathbf{f}(\mathbf{k}, \mathbf{r}) = U(\mathbf{k}, \mathbf{r}) \begin{pmatrix} f_{\uparrow}(\mathbf{k}, \mathbf{r}) & 0 \\ 0 & f_{\downarrow}(\mathbf{k}, \mathbf{r}) \end{pmatrix} U^{\dagger}(\mathbf{k}, \mathbf{r}) \quad (27)$$

in terms of the scalar occupancy functions for up and down spins and the spinor rotation matrix

$$U(\mathbf{k}, \mathbf{r}) = \begin{pmatrix} \cos(\theta/2)e^{-i\phi/2} & -\sin(\theta/2)e^{-i\phi/2} \\ \sin(\theta/2)e^{i\phi/2} & \cos(\theta/2)e^{i\phi/2} \end{pmatrix}. \quad (28)$$

We have suppressed the $\mathbf{k}$ and $\mathbf{r}$ dependence of θ and ϕ for simplicity.

Elsewhere, we have solved the Boltzmann equation to find $\mathbf{f}(\mathbf{k},\mathbf{r})$ for a typical spin-transfer geometry.[22] For the simple scattering problem treated here, the reflected and transmitted distributions are determined entirely by the reflection and transmission amplitudes and the incident electron distribution at the interface between the non-magnet and the ferromagnet: $\mathbf{f}(\mathbf{k}) = \mathbf{f}(x = 0, \mathbf{k})$. For this distribution, the semi-classical version of the spin current (6) is

$$\mathbf{Q}^{\mathrm{in}} = \frac{\hbar}{2} \int\limits_{v_x > 0} \frac{d^3k}{(2\pi)^3} \mathrm{Tr}\left[\mathbf{f}(\mathbf{k})\boldsymbol{\sigma}\right] \otimes \mathbf{v}(\mathbf{k}). \quad (29)$$

The restriction $v_x > 0$ limits the integration to the occupied electron states that move toward the interface. Using (27), (28) and the cyclic properties of the trace, we get, *e.g.*,

$$Q_{xx}^{\mathrm{in}} = \frac{\hbar}{2} \int\limits_{v_x > 0} \frac{d^3k}{(2\pi)^3} f_{\mathrm{p}}(\mathbf{k}) v_x(\mathbf{k}) \sin\theta_{\mathbf{k}} \cos\phi_{\mathbf{k}}, \quad (30)$$

where $f_{\mathrm{p}}(\mathbf{k}) = f_{\uparrow}(\mathbf{k}) - f_{\downarrow}(\mathbf{k})$ determines the degree of polarization at each point on the Fermi surface. The angles $\theta_{\mathbf{k}}$ and $\phi_{\mathbf{k}}$ determine the direction of the spin polarization. Electron states in the immediate vicinity of the Fermi surface dominate the transport of charge and spin. Therefore, we write

$$f_{\sigma}(\mathbf{k}) \rightarrow f_0(\epsilon_{\mathbf{k}}) + g_{\sigma}(\mathbf{q}) \frac{\partial f_0(\epsilon_{\mathbf{k}})}{\partial \epsilon_{\mathbf{k}}} \quad (31)$$

where f_0 is the equilibrium Fermi-Dirac distribution function and the partial derivative restricts $\mathbf{k}$ to the

Fermi surface. We write $g_\sigma(\mathbf{q})$ rather than $g_\sigma(\mathbf{k})$ because $|\mathbf{k}|^2 = k_x^2 + q^2 = k_F^2$. The equilibrium term does not contribute to the spin current. Otherwise, we let $d^3k = d^2q\,dk_x$ and use $\int dk_x \partial f_0/\partial \epsilon_\mathbf{k} = 1/\hbar|v_x(\mathbf{q})|$ in (30). The result is

$$Q_{xx}^{\mathrm{in}} = \frac{1}{4\pi} \int\limits_{v_x>0} \frac{d^2q}{(2\pi)^2} g_\mathrm{p}(\mathbf{q}) \sin\theta_\mathbf{q} \cos\phi_\mathbf{q} \qquad (32)$$

where

$$g_\mathrm{p}(\mathbf{q}) = g_\uparrow(\mathbf{q}) - g_\downarrow(\mathbf{q}). \qquad (33)$$

For Q_{yx}^{in}, change $\cos\phi_\mathbf{q}$ to $\sin\phi_\mathbf{q}$ in (32).

The reflected spin current due to all the conduction electrons is

$$\mathbf{Q}^{\mathrm{ref}}(\mathbf{r}) = \frac{\hbar}{2} \int\limits_{v_x>0} \frac{d^3k}{(2\pi)^3} \mathrm{Tr}\left[\mathbf{R}^\dagger(\mathbf{k},\mathbf{r})\mathbf{f}(\mathbf{k})\mathbf{R}(\mathbf{k},\mathbf{r})\boldsymbol{\sigma}\right] \otimes \mathbf{v}^{\mathrm{ref}}(\mathbf{k}) \qquad (34)$$

where

$$\mathbf{R}(\mathbf{k}) = \begin{pmatrix} R_\uparrow(\mathbf{k})e^{i\mathbf{k}\cdot\mathbf{r}} & 0 \\ 0 & R_\downarrow(\mathbf{k})e^{i\mathbf{k}\cdot\mathbf{r}} \end{pmatrix} \qquad (35)$$

and $\mathbf{v}^{\mathrm{ref}}(\mathbf{k})$ is the velocity of a reflected electron with wave vector $\mathbf{k}$. The $\mathbf{r}$-dependent phase factors in (35) cancel out in (34) so, e.g.,

$$Q_{xx}^{\mathrm{ref}} = -\frac{1}{4\pi} \int\limits_{v_x>0} \frac{d^2q}{(2\pi)^2} g_\mathrm{p}(\mathbf{q}) \sin\theta_\mathbf{q} \left|R_\uparrow^*(\mathbf{q})R_\downarrow(\mathbf{q})\right| \mathrm{Re}\left[e^{-i(\phi_\mathbf{q}-\Delta\phi_\mathbf{q})}\right] \qquad (36)$$

where $\Delta\phi_\mathbf{q}$ is the relative phase of the reflection amplitude as in (25). For Q_{yx}^{ref}, change Re to Im in (36).

Finally, the total transmitted spin current is

$$\mathbf{Q}^{\mathrm{tr}}(\mathbf{r}) = \frac{\hbar}{2} \int\limits_{v_x>0} \frac{d^3k}{(2\pi)^3} \mathrm{Tr}\left[\mathbf{T}^\dagger(\mathbf{k},\mathbf{r})\mathbf{f}(\mathbf{k})\mathbf{T}(\mathbf{k},\mathbf{r})\boldsymbol{\sigma}\right] \otimes \mathbf{v}^{\mathrm{tr}}(\mathbf{k}) \qquad (37)$$

where

$$\mathbf{T}(\mathbf{k},\mathbf{r}) = \begin{pmatrix} T_\uparrow(\mathbf{k})e^{i\mathbf{k}^\uparrow\cdot\mathbf{r}} & 0 \\ 0 & T_\downarrow(\mathbf{k})e^{i\mathbf{k}^\downarrow\cdot\mathbf{r}} \end{pmatrix} \qquad (38)$$

and

$$\mathbf{v}^{\mathrm{tr}}(\mathbf{k}) = \frac{\mathbf{v}^\uparrow(\mathbf{k}) + \mathbf{v}^\downarrow(\mathbf{k})}{2}. \qquad (39)$$

In these formulae, the wave vector for incident states, $\mathbf{k}$, transforms to either $\mathbf{k}^\uparrow$ or $\mathbf{k}^\downarrow$ when the electron enters the ferromagnet. The average transmitted velocity $\mathbf{v}^{\mathrm{tr}}(\mathbf{k})$ is defined only at values of $\mathbf{q}$ where both spins transmit. A comparison of, say,

$$Q_{xx}^{\mathrm{tr}}(x) = \frac{1}{4\pi} \int\limits_{v_x>0} \frac{d^2q}{(2\pi)^2} g_\mathrm{p}(\mathbf{q}) \sin\theta_\mathbf{q} \frac{v_x^\uparrow(\mathbf{q}) + v_x^\downarrow(\mathbf{q})}{|2v_x(\mathbf{q})|} \mathrm{Re}\left[T_\uparrow^*(\mathbf{q})T_\downarrow(\mathbf{q})e^{-i\phi_\mathbf{q}}e^{-i(k_x^\uparrow-k_x^\downarrow)x}\right] \qquad (40)$$

with (24) confirms that (37) is correct with the definitions (38) and (39). For Q_{yx}^{tr}, change Re to Im in (40).

At this point, we must make a specific choice for $g_\mathrm{p}(\mathbf{k})$ and the polarization of the incident spin current. Let us assume the current is completely spin polarized along $+\hat{\mathbf{x}}$. This fixes $\theta_\mathbf{k} = \pi/2$ and $\phi_\mathbf{k} = 0$. For the distribution (33), we begin with the approximate form

$$g_\mathrm{p}(\mathbf{q}) = a + bv_x(\mathbf{q}). \qquad (41)$$

The two terms account for interface and bulk effects, respectively. The velocity-dependent bulk term is familiar from textbook treatments of electrical conductivity[28] except, from (11), gradients in spin accumulation (rather than electric potential) drive the spin current in the non-magnet. The constant term is needed because a spin-dependent chemical

potential difference $\Delta\mu$ across an interface also drives a spin current.[17] In this paper, we assume that the interface resistance is large (large reflection probability) so we use

$$g_{\mathrm{p}}(\mathbf{q}) \simeq a = \Delta\mu. \tag{42}$$

This is the same approximation that is made in Landauer-type transport calculations.[19–21]

With these choices, the incident spin current is

$$Q_{xx}^{\mathrm{in}} = \frac{1}{2}\frac{1}{(2\pi)^2}\int_0^{k_{\mathrm{F}}} dq\, q\Delta\mu = \frac{1}{4}\frac{k_{\mathrm{F}}^2}{(2\pi)^2}\Delta\mu. \tag{43}$$

The reflected spin currents normalized to the incident spin current are

$$\frac{Q_{xx}^{\mathrm{ref}}}{Q_{xx}^{\mathrm{in}}} = -\frac{2}{k_{\mathrm{F}}^2}\int_0^{k_{\mathrm{F}}} dq\, q|R_\uparrow^*(q)R_\downarrow(q)|\cos\Delta\phi_{\mathrm{q}} \tag{44}$$

and

$$\frac{Q_{yx}^{\mathrm{ref}}}{Q_{xx}^{\mathrm{in}}} = -\frac{2}{k_{\mathrm{F}}^2}\int_0^{k_{\mathrm{F}}} dq\, q|R_\uparrow^*(q)R_\downarrow(q)|\sin\Delta\phi_{\mathrm{q}}. \tag{45}$$

We get $Q_{yx}^{\mathrm{ref}} \neq 0$ because, as discussed earlier, many of the spins rotate upon reflection. On the other hand, the sinusoidal factors lead to substantial self-cancellation of the integrals (44) and (45) when the range of $\Delta\phi_{\mathrm{q}}$ is large (see bottom panel of Figure 3).[23] In most cases, we find the total transverse reflected spin current to be very small.

The normalized transmitted spin currents are

$$\frac{Q_{xx}^{\mathrm{tr}}(x)}{Q_{xx}^{\mathrm{in}}} = \frac{2}{k_{\mathrm{F}}^2}\int_0^{k_{\mathrm{F}}^\downarrow} dq\, q\frac{k_x^\downarrow(q) + k_x^\uparrow(q)}{2|k_x(q)|}T_\uparrow(q)T_\downarrow(q)\cos\left[(k_x^\downarrow(q) - k_x^\uparrow(q))x\right] \tag{46}$$

and

$$\frac{Q_{yx}^{\mathrm{tr}}(x)}{Q_{xx}^{\mathrm{in}}} = \frac{2}{k_{\mathrm{F}}^2}\int_0^{k_{\mathrm{F}}^\downarrow} dq\, q\frac{k_x^\downarrow(q) + k_x^\uparrow(q)}{2|k_x(q)|}T_\uparrow(q)T_\downarrow(q)\sin\left[(k_x^\downarrow(q) - k_x^\uparrow(q))x\right]. \tag{47}$$

Based on the behavior of the transverse reflected spin current, we expect (46) and (47) to decay as a function of x because the generally wide range of $\Delta k = k_x^\downarrow(q) - k_x^\uparrow(q)$ (see top panel of Figure 3) ought to induce self-cancellation of the integrals. In fact, like a similar integral that appears in the theory of oscillatory exchange coupling,[29] we can extract the asymptotic form ($x \to \infty$) analytically using a stationary phase approximation. Only small values of q contribute in that instance so for, say, the xx component, we find

$$\lim_{x\to\infty}\frac{Q_{xx}^{\mathrm{tr}}(x)}{Q_{xx}^{in}} = -2\frac{k_{\mathrm{F}}^\uparrow k_{\mathrm{F}}^\downarrow}{k_{\mathrm{F}}^2}\frac{k_{\mathrm{F}}^\downarrow + k_{\mathrm{F}}^\uparrow}{2k_{\mathrm{F}}}T_\uparrow(0)T_\downarrow(0)\frac{\sin\left[(k_{\mathrm{F}}^\uparrow - k_{\mathrm{F}}^\downarrow)x\right]}{(k_{\mathrm{F}}^\uparrow - k_{\mathrm{F}}^\downarrow)x}. \tag{48}$$

To understand this result, we note (see the top panel of Fig. 3) that the electron states with wave vectors in an interval δq near $q = 0$ (which share the value $\Delta k \simeq k_{\mathrm{F}}$) play a special role. These states precess together (coherently) with spatial frequency $k_{\mathrm{F}}^\uparrow - k_{\mathrm{F}}^\downarrow$. Slow dephasing begins only after a distance x where $x\delta q \sim 1$.

The oscillatory, algebraic decay exhibited by (48) contrasts markedly with the assumption of monotonic, exponential decay made by others.[2,13,30] Of course, incoherent scattering processes may be expected to superimpose an exponential decay on the algebraic decay we find. The solid curves in Fig. 4 illustrate the behavior of the transmitted spin current (46) for three free-electron models. The dashed curves show the asymptotic behavior from

(48). The top panel corresponds to Fig. 3 where the Fermi sphere of the non-magnet is significantly smaller than the majority sphere and significantly larger than the minority sphere. The middle panel is a situation where the Fermi sphere of the non-magnet is identical in size to the majority sphere and both are significantly larger than the minority sphere. Finally, the lower panel shows results for majority and minority spheres which are, respectively, slightly larger and slightly smaller than the Fermi sphere of the non-magnet. This corresponds to the so-called "s-d model" where the conduction electrons bands in the ferromagnet are regarded as slightly split by exchange with localized moments.

The interfacial "spin-filter" makes each solid curve in Fig. 4 differ from unity already at $x = 0$. The filter is most effective when the Fermi surface of the non-magnet is poorly matched with one or both of the Fermi surfaces of the ferromagnet. Owing to (18), this is consistent with our earlier discussion where we identified the transmission probability condition $T^\uparrow(q) \neq T^\downarrow(q)$ as a prerequisite to the action of the spin filter. The subsequent decay of each curve in Fig. 4 to zero reflects the distribution of spatial precession frequencies as we have indicated. We have repeated these calculations assuming that the distribution function g_p is proportional to the velocity term in (41) alone rather than the constant term in (41) alone. We find no significant changes from the results of Fig. 4.

We are now ready to use our computed results to find the spin-transfer torque (14) for free electron models. The top and bottom panels of Figure 5 show the transverse spin space vectors $\mathbf{N}$, $\mathbf{Q}^{\text{in}} \cdot \hat{\mathbf{x}}$, $\mathbf{Q}^{\text{ref}} \cdot \hat{\mathbf{x}}$, and $\mathbf{Q}^{\text{tr}} \cdot \hat{\mathbf{x}}$ for the Fermi surfaces used in the top and bottom panels of Fig. 4. We have suppressed the contraction with $\hat{\mathbf{x}}$ in the spin current labels for clarity. In fact, the vectors for $\mathbf{Q}^{\text{ref}}$ and $\mathbf{Q}^{\text{tr}}$ represent these quantities just at the interface. Therefore, the reflected piece includes the dephasing effects of differential spin rotation whereas the transmitted piece does *not* include the dephasing effects of differential spin precession. As we have seen, the latter reduces the transmitted spin torque to zero not far from the interface. Therefore, we have drawn the torque vector (for a unit area of interface) so $\mathbf{N} = \mathbf{Q}^{\text{in}} + \mathbf{Q}^{\text{ref}}$. The top panel of Fig. 5 (large Fermi surface mismatch) shows a significant dephasing of the reflected spin current. The bottom panel of Fig. 5 (small Fermi surface mismatch) shows nearly zero reflected spin current. The reflected spin current is exactly zero for the model (not shown) used in the middle panel of Fig. 4. These results show that, unless the Fermi surface mismatch is very small, the interface effectively absorbs the entire transverse component of incident spin current. This abrupt change in angular momentum is the source of current-induced spin-transfer torque at the interface between a ferromagnet and a non-magnet.

The dashed arc labeled Q^{sf} in each panel of Fig. 5 is a portion of a circle whose center is the "tail" position for all three spin current vectors. The radius of this circle, compared to the length of the vector $\mathbf{Q}^{\text{in}}$, gives
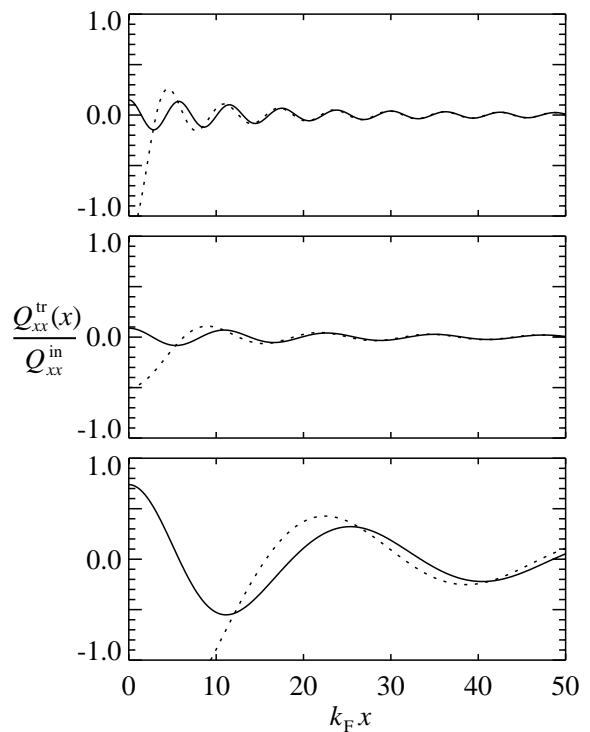

FIG. 4: Decay of transverse transmitted spin current as a function of distance from the interface for three free electron models. In each panel, the solid curve is the exact result (46) and the dashed curve is the asymptotic result (48). Top panel: the mismatch is very large between the sizes of the magnetic and non-magnetic Fermi surfaces; $k_{F\uparrow}/k_F = 1.5$ and $k_{F\downarrow}/k_F = 0.5$. This is the model used in Fig. 3. Middle panel: the Fermi surfaces are identical for the non-magnet and the majority electrons in the magnet; $k_{F\uparrow}/k_F = 1.0$ and $k_{F\downarrow}/k_F = 0.5$. Bottom panel: an s-d-like model where the mismatch is very small between the sizes of the magnetic and non-magnetic Fermi surfaces: $k_{F\uparrow}/k_F = 1.1$ and $k_{F\downarrow}/k_F = 0.9$.

an indication of the magnitude of the spin filter effect. Quantitatively, the circle radius is proportional to

$$\frac{Q_x^{\text{sf}}}{Q_{xx}^{\text{in}}} = \frac{2}{k_F^2} \int_0^{k_F} dq\, q \left| R_\uparrow^*(q) R_\downarrow(q) \right|$$

$$+ \frac{2}{k_F^2} \int_0^{k_F^\downarrow} dq\, q \frac{k_x^\downarrow(q) + k_x^\uparrow(q)}{2|k_x(q)|} \left| T_\uparrow(q) T_\downarrow(q) \right| . \quad (49)$$

With this definition, Q^{sf} measures the magnitude of the total outgoing spin current (reflected plus transmitted) without taking phase cancellation into account. This scalar measure of the spin filter is truly meaningful only when the reflection and transmission amplitudes are both real and positive, which is not the case. Nevertheless, the dashed arcs give some insight into the efficacy of the spin filter mechanism for different free-electron Fermi surfaces.

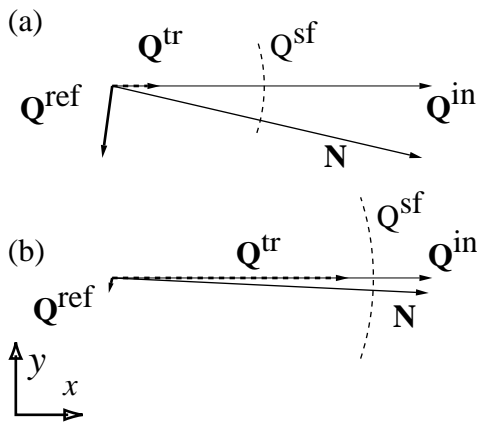The foregoing makes clear that free electron models

FIG. 5: Graphical representation of the interfacial torque and transverse spin currents for two free electron models. The x-components are horizontal and y-components are vertical. The horizontal arrow is the incident spin current directed along the x-direction. The dashed arc indicates the reduction in spin current due to the "spin-filter" effect. The thick arrow is the reflected spin current at $x = 0$. The dashed arrow is the transmitted spin current at $x = 0$. The thin arrow is the final torque taking account of the fact that precessional averaging in the ferromagnet drives $\mathbf{Q}^{\mathrm{tr}} \to 0$ after a few lattice constants. Panel (a) is the large Fermi surface mismatch model of Fig. 3. Panel (b) is the s-d model of the bottom panel of Fig. 4.

are useful for building intuition about spin currents and spin-transfer torque. However, there is no substitute for first-principles calculations if we are interested in specific material interfaces. At the very least, such calculations can be used to judge the correctness of approximate constructs such as the s-d model.

IV.   REAL INTERFACES

In this section we repeat the calculations of Section III B for ten lattice-matched interfaces between a non-magnet and a ferromagnet using a more realistic model of the electronic structure for both. Specifically, we calculate the transmission and reflection amplitudes using a linearized-augmented-plane-wave implementation of the local-spin-density approximation. The details can be found in Ref. 31 and Ref. 32. Compared to that earlier work, the calculations reported here use a mesh in reciprocal space that is a factor of two denser in each direction. For one case (Co/Cu), we checked that no changes in relative spin currents greater than 10^{-3} occurred when the mesh was made another 2×2 denser. Evanescent states (which decay exponentially away from the interface) play a crucial role in the calculation of the reflection and transmission amplitudes. We have ignored them in our spin currents computations. Their effect is to change the wave functions in the immediate vicinity (a few atomic layers) of the interface in such a way that there is no true discontinuity in the transverse spin current at the interface. As a practical matter, this means only that the "interfacial" torque we compute is–in reality–spread out over a few atomic spacings.

The two middle panels of Fig. 6 show a slice through the Fermi surface of copper and the same slice through the majority (dashed lines) and minority (solid) Fermi surfaces of cobalt for the Co/Cu(111) system. The Fermi surface topologies here are much more complicated than the corresponding free electron topologies (cf. Fig. 3). Moreover, as the Co minority Fermi surface shows, there can be more than one pair of states for each parallel wave vector. Consequently, we supplement every integral over parallel wave vectors with a sum over all possible states that move toward the interface for each parallel wave vector. We index these states by n, refer to them as associated with the nth sheet of the Fermi surface, and adopt the notation $\mathbf{k}_{n\sigma} = \{\mathbf{q}, k_{n\sigma}^x\}$ to label Fermi surface wave functions. We drop the spin index σ in the non-magnet.

The transverse pieces of the incident spin current for a real interface are

$$Q_{xx}^{\mathrm{in}} = \frac{1}{4\pi} \int \frac{d^2q}{(2\pi)^2} \sum_n g_{\mathrm{p}}(\mathbf{k}_n) \sin\theta(\mathbf{k}_n) \cos\phi(\mathbf{k}_n) \tag{50}$$

and

$$Q_{yx}^{\mathrm{in}} = \frac{1}{4\pi} \int \frac{d^2q}{(2\pi)^2} \sum_n g_{\mathrm{p}}(\mathbf{k}_n) \sin\theta(\mathbf{k}_n) \sin\phi(\mathbf{k}_n). \tag{51}$$

These differ from the corresponding free electron formulae by the sum over the sheet index n. That sum is restricted to the sheets of the Fermi surface where the electrons move *toward* the interface.

As before, the efficacy of the spin filter can be judged from the interface transmission and reflection probabilities. These state-to-state ($n \to n'$) quantities are

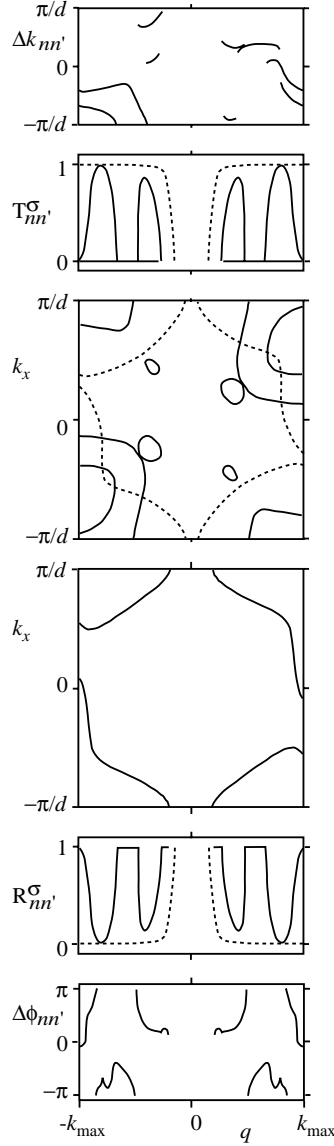$$\mathrm{T}_{nn'}^{\sigma} = \frac{v_{n'}^{\sigma}}{v_n} |T_{\sigma nn'}|^2 \tag{52}$$

FIG. 6: Same as Fig. 3 for a real material interface: Co/Cu(111) with parallel wave vectors in the [1$\bar{1}$0] direction. The two middle panels show the Fermi surface for the non-magnet and the superimposed Fermi surfaces of the majority (dashed) and minority (solid) states of the ferromagnet. The panel just above the magnetic Fermi surfaces is the probability for transmission into the ferromagnet for majority (dashed) and minority (solid) electrons. The panel just below the non-magnetic Fermi surface is the probability for reflection back into the non-magnet for majority (dashed) and minority (solid) electrons. The bottom panel shows the phase in (56) acquired by an electron because its spin rotates upon reflection. The top panel shows the wave vector difference (63) for a transmitted electron.

and

$$\mathrm{R}_{nn'}^{\sigma} = \frac{|v_{n'}|}{v_n} \left| R_{\sigma nn'} \right|^2 . \tag{53}$$

The absolute value is needed in (53) because $v_{n'} < 0$ and $\mathrm{R}_{nn'}^{\sigma}$ must be non-negative. Fig. 6 shows the transmission and reflection probabilities for one slice through the Co/Cu(111) Fermi surfaces.

The transverse components of the reflected spin current are

$$Q_{xx}^{\mathrm{ref}} = -\frac{1}{4\pi} \int \frac{d^2 q}{(2\pi)^2} \sum_n g_{\mathrm{P}}(\mathbf{k}_n) \sin\theta(\mathbf{k}_n) \sum_{n'} \frac{|v_x(\mathbf{k}_{n'})|}{|v_x(\mathbf{k}_n)|} \mathrm{Re}\left[R_{\uparrow nn'}^* R_{\downarrow nn'} e^{-i\phi(\mathbf{k}_n)} \right] \tag{54}$$

and

$$Q_{yx}^{\text{ref}} = -\frac{1}{4\pi} \int \frac{d^2q}{(2\pi)^2} \sum_n g_{\text{p}}(\mathbf{k}_n) \sin\theta(\mathbf{k}_n) \sum_{n'} \frac{|v_x(\mathbf{k}_{n'})|}{|v_x(\mathbf{k}_n)|} \text{Im}\left[R_{\uparrow nn'}^* R_{\downarrow nn'} e^{-i\phi(\mathbf{k}_n)}\right]. \tag{55}$$

Here, the sum over n' is restricted to the sheets of the Fermi surface where the electrons move *away* from the interface. Similar to the free electron case, the dephasing of the reflected transverse spin current is determined by reflection phases $\Delta\phi_{nn'}^{\text{R}}(\mathbf{q})$ where

$$R_{\uparrow nn'}^* R_{\downarrow nn'} = \left|R_{\uparrow nn'}^* R_{\downarrow nn'}\right| e^{i\Delta\phi_{nn'}^{\text{R}}(\mathbf{q})}. \tag{56}$$

The bottom panel of Fig. 6 shows that the Co/Cu(111) phases are both more complicated and exhibit greater dispersion than the corresponding free electron results plotted in Fig. 3.

The transverse pieces of $\mathbf{Q}^{\text{in}}$ and $\mathbf{Q}^{\text{ref}}$ written above are closely related to the *mixing conductance*, G_{mix}, introduced by Brataas *et al.*[19] and computed recently by Xia *et al.*[23] In our notation,

$$G_{\text{mix}} = \frac{e^2}{h} A \int \frac{d^2q}{(2\pi)^2} \sum_n \left[1 - \sum_{n'} \frac{|v_x(\mathbf{k}_{n'})|}{|v_x(\mathbf{k}_n)|} R_{\uparrow nn'}^* R_{\downarrow nn'}\right]. \tag{57}$$

This formula is relevant to situations where $g_{\text{p}}(\mathbf{k}_n)$, $\theta(\mathbf{k}_n)$, and $\phi(\mathbf{k}_n)$ in (50)-(55) are all constants–a restriction implicit in the Landauer description of transport. In that case, the real and imaginary parts of G_{mix} are proportional to the xx and yx components of $\mathbf{Q}^{\text{in}} + \mathbf{Q}^{\text{ref}}$. From (14), the latter is proportional to the spin-transfer torque if we neglect the transverse part of the transmitted spin current.[19,22] For the systems treated by both of us, our numerical results for spin-transfer torque agree semi-quantitatively with the mixing conductance calculations of Xia at al.

The transverse transmitted spin currents are

$$Q_{xx}^{\text{tr}}(x) = \frac{1}{4\pi} \int \frac{d^2q}{(2\pi)^2} \sum_n g_{\text{p}}(\mathbf{k}_n) \frac{\sin\theta(\mathbf{k}_n)}{|v_x(\mathbf{k}_n)|} \text{Re}\left[e^{-i\phi(\mathbf{k}_n)} \sum_{n'',n'} T_{\uparrow nn''}^* T_{\downarrow nn'} \Phi_{n''n'}(\mathbf{q},x) e^{i(k_{n''\uparrow}^x - k_{n'\downarrow}^x)x}\right] \tag{58}$$

and

$$Q_{yx}^{\text{tr}}(x) = \frac{1}{4\pi} \int \frac{d^2q}{(2\pi)^2} \sum_n g_{\text{p}}(\mathbf{k}_n) \frac{\sin\theta(\mathbf{k}_n)}{|v_x(\mathbf{k}_n)|} \text{Im}\left[e^{-i\phi(\mathbf{k}_n)} \sum_{n'',n'} T_{\uparrow nn''}^* T_{\downarrow nn'} \Phi_{n''n'}(\mathbf{q},x) e^{-i(k_{n''\uparrow}^x - k_{n'\downarrow}^x)x}\right]. \tag{59}$$

Apart from the sums over n' and n'' (both restricted to sheets of the ferromagnetic Fermi surfaces where electrons move away from the interface), these formula are less simple than the corresponding free electron results (46) and (47) for two reasons. First, the transmission amplitudes, $T_{\sigma nn'}$, are complex rather than real. Second, the Bloch wave functions $\psi_\sigma(\mathbf{R}, x, \mathbf{k}_{n\sigma})$ have a non-trivial dependence on the spatial variable $\mathbf{R}$ parallel to the interface plane. For the latter reason, the transmitted spin currents contain a factor $\Phi_{n''n'}(\mathbf{q}, x)$ defined by

$$\Phi_{nn'}(\mathbf{q},x)e^{-i(k_{n\uparrow}^x - k_{n'\downarrow}^x)x} = \frac{1}{2A} \int_{v_x>0} d\mathbf{R} \left[\psi_\uparrow^*(\mathbf{r}, \mathbf{k}_{n\uparrow})\hat{v}_x\psi_\downarrow(\mathbf{r}, \mathbf{k}_{n'\downarrow}) - \psi_\downarrow(\mathbf{r}, \mathbf{k}_{n'\downarrow})\hat{v}_x\psi_\uparrow^*(\mathbf{r}, \mathbf{k}_{n\uparrow})\right]. \tag{60}$$

This yields

$$\Phi_{nn'}(\mathbf{q},x) = \frac{v_x^{n'\downarrow} + v_x^{n'\downarrow}}{2} \tag{61}$$

when free electron wave functions are used in (60). Otherwise, $\Phi_{n''n'}(\mathbf{q}, x)$ is a complex, periodic function of x with period equal to one layer spacing. Thus, it can be calculated once and propagated from layer to layer. A related factor enters the reflected spin currents (58) and (59). However, because the spin up and spin down wave functions are the same in the non-magnet, it reduces to the velocity factor in the numerator of those expressions.

Given the foregoing, it is sensible to define transmission phases $\Delta\phi_{nn'}^{\text{T}}(\mathbf{q})$ so that

$$T_{\uparrow nn'}^* T_{\downarrow nn'} \Phi_{n''n'}(\mathbf{q}, x=0) = \left|T_{\uparrow nn'}^* T_{\downarrow nn'} \Phi_{n''n'}(\mathbf{q}, x=0)\right| e^{i\Delta\phi_{nn'}^{\text{T}}(\mathbf{q})}. \tag{62}$$

This tells us that, unlike free electrons, the spins of Bloch electrons generally rotate when they transmit through a real material interface. If the distribution of transmission phases is broad, substantial cancellation of the transmitted spin current occurs at $x = 0$ when we sum over all transmitted electrons. This effect is independent of the spin filter, which also acts at $x = 0$.

Any spin current that survives to propagate into the ferromagnet rapidly disappears due to differential spa-

tial precession. The (generalized) spatial precession frequency is determined by the difference in wave vector for different sheets of the majority and minority Fermi surfaces:

$$\Delta k_{n'n''} = k^x_{n'\downarrow} - k^x_{n''\uparrow}. \tag{63}$$

The top panel of Fig. 6 illustrates the distribution of $\Delta k_{n'n''}$ for a Fermi surface slice of Co/Cu(111). The large dispersion seen there suggests that the spin current decays very quickly in the ferromagnet. This is confirmed by Fig. 7, which shows the computed decay of the transverse spin current for three interface orientations of Co/Cu. The non-zero value of the dashed curves at $x = 0$ shows that a large amount of rotation occurs upon transmission. The Fermi surfaces are more complicated than the free electron models, so the initial decay is more complicated also. Nevertheless, both the (111) and (110) orientations settle into behavior that is readily characterized as a damped precession. The amplitude of the precession for the (100) orientation is so small that it is difficult to see whether it is precessing or not. In general, there could be several decaying precessions with different precession rates and different amplitudes.

It is worth noting that none of these curves (or analogous curves for the other material pairs we have studied) resembles the the bottom panel of Fig. 4 appropriate to the s-d model. This lack of agreement is consistent with the fact that essentially *all* the Fermi surface wave functions in third-row ferromagnets contain more "localized" $3d$ character than "delocalized" $4s$ character.[33]

Figure 8 graphically summarizes our first-principles spin current calculations for ten different interface combinations. The vectors labeled $\mathbf{Q}^{\text{ref}}$ and $\mathbf{Q}^{\text{tr}}$ correspond to $x = 0$ and reflect the effect of spin filtering and spin rotation only. $\mathbf{Q}^{\text{ref}}$ is very small and, as we have emphasized, $\mathbf{Q}^{\text{tr}} \to 0$ after a few lattice constants. Therefore, the torque per unit area of interface is $\mathbf{Q}^{\text{in}} + \mathbf{Q}^{\text{ref}} \simeq \mathbf{Q}^{\text{in}}$. Due to spin filtering, differential spin rotation, and differential precession, nearly all of the incident transverse spin current is absorbed in the immediate vicinity of the interface. For Co/Cu, Fe/Ag, and Fe/Au, the spin-filter accounts for somewhat more than half of the effect and the interface dephasing for the rest. For Ni/Cu and Fe/Cr the spin filter effect is weaker. For Ni/Cu, the decay of the precessing transmitted spin current plays a large role.

Of course, our calculations pertain to ideal, lattice-matched interfaces. A variety of effects make the interfacial absorption of transverse spin even more efficient. We have mentioned already that scattering in the ferromagnetic layer increases the rate of decay of the precession. Steps at the interface lead to increased dephasing for both reflection and transmission. For thin layers where the decay of the precession might not be complete, the dephasing on passing through the second interface generally leads to a further decay of the transverse spin current. Thickness fluctuations further reduce the spin current.

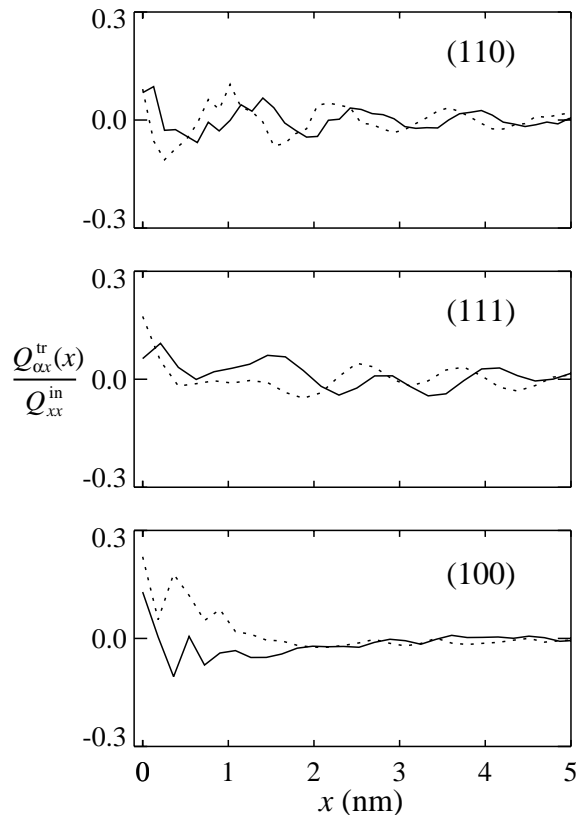The interface torque we compute is interesting because

FIG. 7: Decay of transverse transmitted spin current as a function of distance from the interface for three orientations of Co/Cu. For a unit incident transverse polarization, the solid curve in each panel is $Q_{xx}(x)$. The dashed curve in each panel is $Q_{yx}(x)$.

of the recent demonstrations of current-induced magnetization switching.[5,6] However, the material pair that optimizes the switching is not determined by the conversion of the spin current into a torque. This process is the same for all of the interfaces considered. For the ideal interfaces considered here, the optimum choice depends on the ability of the material pair to generate a spin current in the first place. This depends on the spin-dependent interface resistances and the spin-dependent bulk conductivities. The Fe/Au and Fe/Ag pairs have the strongest spin dependence of the interface resistance.[34] However, in reality the optimum combination will likely depend on growth considerations. The general mismatch between the body-centered-cubic Fe lattice and the face-centered-cubic Au or Ag lattice will probably lead to poor growth, unless the interface is forced to be (100) (where the rotated lattices match quite well) and the number of steps at the interface is kept quite small.

V. SUMMARY

In this paper, we used free electron models and first principles electronic structure calculations to study the
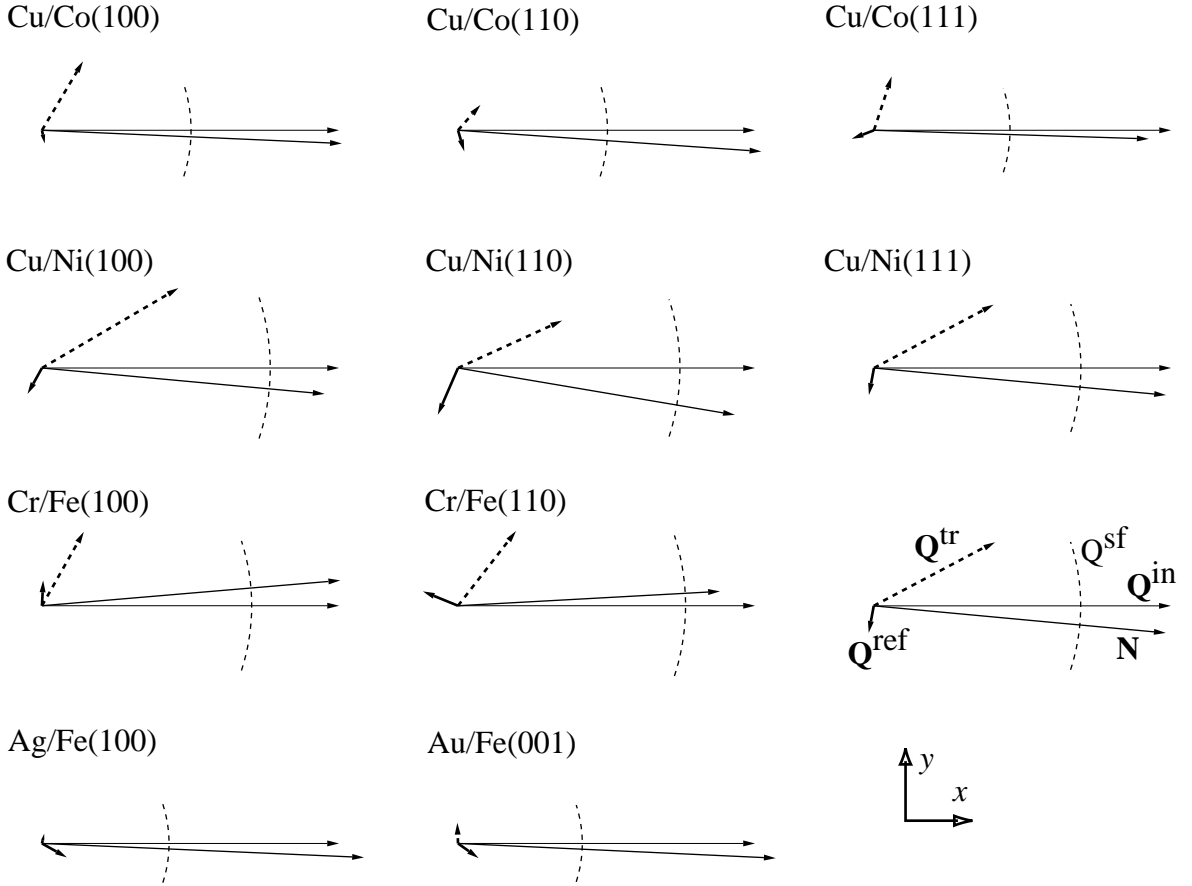
FIG. 8: Graphical representation of the interfacial torque and transverse spin currents for a series of real interfaces. The x-components are horizontal and y-components are vertical. The horizontal arrow is the incident spin current directed along the x-direction. The dashed arc indicates the reduction in spin current due to the "spin-filter" effect. The thick arrow is the reflected spin current at $x = 0$. The dashed arrow is the transmitted spin current at $x = 0$. The thin arrow is the final torque taking account of the fact that precessional averaging in the ferromagnet drives $\mathbf{Q}^{tr} \rightarrow 0$ after a few lattice constants.

spin-transfer torque that occurs when a spin-polarized current flows from a non-magnet into a ferromagnet through a perfect interface. The origin of the torque is a transfer of spin angular momentum from the conduction electrons to the magnetization of the ferromagnet. The origin of the angular momentum transfer is the absorption of transverse spin current by the interface. We identified three distinct processes that contribute to the absorption: (1) spin-dependent reflection and transmission; (2) rotation of reflected and transmitted spins; and (3) spatial precession of spins in the ferromagnet. When summed over all Fermi surface electrons, these processes reduce the transverse component of the transmitted and reflected spin currents to nearly zero for most systems of interest. Therefore, to a good approximation, the torque on the magnetization is proportional to the transverse piece of the incoming spin current.

To be more quantitative, we used the analogy between charge current and spin current to show that a spin current flowing in the $+\hat{\mathbf{x}}$ direction (perpendicular to the interface) delivers a torque per unit area

$$\frac{\mathbf{N}_c}{A} = (\mathbf{Q}^{in} - \mathbf{Q}^{tr} + \mathbf{Q}^{ref}) \cdot \hat{\mathbf{x}} \qquad (64)$$

to a microscopically small region around the interface. Here, $\mathbf{Q}^{in}$, $\mathbf{Q}^{tr}$, and $\mathbf{Q}^{ref}$ are the incident, transmitted, and reflected spin currents computed using incident, transmitted, and reflected wave functions. We found the latter by solving the one-electron stationary-state scattering problem. In the quasi-classical approximation, the total spin current is the sum of contributions from every conduction electron.

Quite generally, the component of $\mathbf{N}_c$ parallel to the ferromagnetic magnetization is zero. This is consistent with our classical intuition. On the other hand, we found that the transverse components of $\mathbf{Q}^{tr}$ and $\mathbf{Q}^{ref}$ relevant to (64) are also zero (or nearly so), except in very exceptional cases. This means that the entire transverse spin current is absorbed (transferred to the magnetization) in the immediate vicinity of the interface. As indicated above, this is so due to spin filtering, differential spin reflection, and differential spin precession.

The spin-filter effect occurs because the wave function for an incident electron with a non-zero spin component transverse to the magnetization spin can always be written as a linear combination of spin-up and spin-down components. Then, because the reflection and transmission amplitudes differ for up and down spins, the up and down spin content of the reflected and transmitted wave functions (which are spatially separated) differ from both each another and from the incident state. The spin currents directly encode this information. As a result, the right side of (64) is non-zero. This is a one-electron effect that operates independently for every electron.

The two other effects that help drive the transverse parts of $\mathbf{Q}^{\mathrm{tr}}$ and $\mathbf{Q}^{\mathrm{ref}}$ to zero occur when we sum over the entire ensemble of conduction electrons. The first arises because the spin of an electron generally rotates when it is reflected or transmitted at the interface between a non-magnet and a ferromagnet. The rotation is non-classical and the amount of rotation differs considerably for electrons with wave vectors from different portions of the Fermi surface. Phase cancellation occurs when we sum over all electrons. In the end, we find that very little remains of the reflected transverse spin current. The cancellation of the transmitted spin current is less dramatic.

Finally, due to exchange splitting, the electrons that transmit into the ferromagnet possess spin-up and spin-down components with the same total energy, E_{F}, but different kinetic energy and so different wave vectors. This implies that each electron spin precesses (in space) as it propagates away from the interface. However, like the spin rotation angles, the spatial precession frequency varies considerably over the Fermi surface. Consequently, rapid dephasing of the transverse spin components of the individual electrons occurs as the conduction electron ensemble propagates into the ferromagnet. The net result is a precessing spin current that damps out algebraically within a few lattice constants of the interface.

Our first principles calculations show that the relative importance of these three mechanisms differs for different materials pairs and also for different crystallographic orientations for the same material pair. Nevertheless, the final result is the same in all cases: the transverse spin current essentially disappears at the interface. The concomitant transfer of angular momentum delivers a torque to the magnetization in the immediate vicinity of the interface.

VI. ACKNOWLEDGMENT

[1] J. C. Slonczewski, J. Magn. Magn. Mater. **159**, L1 (1996); **195**, L261 (1999).

[2] L. Berger, Phys. Rev. B **54**, 9353 (1996); J. Appl. Phys. **81**, 4880 (1997); Phys. Rev. B **59**, 11465 (1999); J. Appl. Phys. **89**, 5521 (2001); *Interaction of electrons with spin-waves in the bulk and in multilayers* cond-mat/0203314.

[3] M. Tsoi, A. G. M. Jansen, J. Bass, W. C. Chiang, M. Seck, V. Tsoi, P. Wyder, Phys. Rev. Lett. **80**, 4281 (1998); J. Z. Sun, J. Magn. Magn. Mater. **202**, 157 (1999); J.-E. Wegrowe, D. Kelly, Ph. Guittienne, Y. Jaccard, and J.-Ph. Ansermet, Europhys. Lett. **45**, 626 (1999).

[4] A. Fert and P. Bruno, in *Ultrathin Magnetic Structure II*, edited by B. Heinrich and J. A. C. Bland (Springer-Verlag, Berlin, 1994).

[5] E. B. Myers, D. C. Ralph, J. A. Katine, R. N. Louie, R. A. Buhrman, Science **285**, 867 (1999); J. A. Katine, F. J. Albert, R. A. Buhrman, E. B. Myers, D. C. Ralph, Phys. Rev. Lett. **84**, 3149 (2000).

[6] J. Grollier, V. Cros, A. Hamzic, J. M. George, H. Jaffrés, A. Fert, G. Faini, J. Ben Youssef, H. Legall, Appl. Phys. Lett. **78**, 3663 (2001).

[7] J.-E. Wegrowe, D. Kelly, T. Truong, Ph. Guittienne, and J.-Ph. Ansermet, Europhys. Lett. **56**, 748 (2001).

[8] W. Weber, S. Rieseen, and H. C. Siegmann, Science **291**, 1015 (2001).

[9] R. Urban, G. Woltersdorf, and B. Heinrich, Phys. Rev. Lett. **87**, 217204 (2001).

[10] G. A. Prinz, J. Mag. Mag. Mat. **200**, 57 (1999).

[11] Ya. B. Bazaliy, B. A. Jones, and S.-C. Zhang, Phys. Rev. B **57**, R3213 (1998); Ya. B. Bazaliy, B.A. Jones, and S.-C. Zhang, J. Appl. Phys. **89**, 6793 (2001); Ya. B. Bazaliy, B. A. Jones, and S.-C. Zhang, *Current-induced magnetization switching in small domains of different anisotropies*, cond-mat/0009034.

[12] J. Z. Sun, Phys. Rev. B **62**, 570 (2000).

[13] C. Heide, P. E. Zilberman, and R. J. Elliott, Phys. Rev. B **63**, 64424 (2001); C. Heide, Phys. Rev. Lett. **87**, 197201 (2001); C. Heide, Phys. Rev. B **65**, 054401 (2001).

[14] J. Miltat, G. Albuquerque, A. Thiaville, and C. Vouille, J. Appl. Phys. **89**, 6982 (2001).

[15] S. Zhang and P. M. Levy, Phys. Rev. B **65**, 052409 (2002).

[16] Y. Tserkovnyak, A. Brataas, and G.E.W. Bauer, *Enhanced Gilbert damping in Thin Ferromagnetic Films*, cond-mat/0110247.

[17] A. G. Aronov, JETP Lett. **24**, 32 (1977); M. Johnson and R. H. Silsbee, Phys. Rev. B **35**, 4959 (1987); P. C. van Son, H. van Kempen, and P. Wyder, Phys. Rev. Lett. **58**, 2271 (1987).

[18] J.-E. Wegrowe, Phys. Rev. B **62**, 1067 (2000).

[19] A. Brataas, Yu. V. Nazarov, and G. E. W. Bauer, Phys. Rev. Lett. **84**, 2481 (2000); A. Brataas, Yu.V. Nazarov, and G. E. W. Bauer, Europhys. Phys. J. B **22**, 99 (2001).

[20] X. Waintal, E. B. Myers, P. W. Brouwer, D. C. Ralph, Phys. Rev. B **62**, 12317 (2000).

[21] D. H. Hernando, Yu.V. Nazarov, A. Brataas, and G. E. W. Bauer, Phys. Rev. B **62**, 5700 (2000).

[22] M.D. Stiles and A. Zangwill, *Non-collinear spin transfer in Co/Cu/Co multilayers*, cond-mat-0110275.

[23] K. Xia, P. J. Kelly, G. E. W. Bauer, A. Brataas, and I. Turek, *Spin Torques in Ferromagnetic/Normal Metal Structures*, cond-mat/0107589.

[24] L. Berger, IEEE Trans. Magn. **31**, 3871 (1995).

[25] Eq. (13) is equivalent to Eq. (10) in [22]. That relation was written in terms of the magnitude of the current. Thus, the term for the reflected spin flux appears there with no minus relative to the transmitted spin flux because the reflected current is in the opposite direction to the transmitted current.

[26] We exploit the fact that the cross section for a time-dependent wave-packet scattering process is determined by the scattering amplitude (here, the transmission and reflection amplitudes) of the corresponding stationary-state, wave-function matching problem. See, *e.g.*, K. Gottfried, *Quantum Mechanics* (Addison-Wesley, Reading, MA, 1966), Section 12.

[27] Spatial precession occurs when a coherent superposition of up and down spin states have the same energy (E_F in this case) but different wave vectors. The more familiar case of temporal precession occurs when a coherent superposition of up and down spin states have the same wave vector but different energies. In both cases, an accumulation of phase changes the orientation of the spin vector.

[28] J. M. Ziman, *Principles of the the theory of solids*, (University Press, Cambridge, 1972), Chapter 7.

[29] M. D. Stiles, Phys. Rev. B**48**, 7238 (1993).

[30] E. Simanek, Phys. Rev. B **63**, 224412 (2001).

[31] M. D. Stiles, J. Appl. Phys. **79**, 5805 (1996).

[32] M. D. Stiles, Phys. Rev. B **54**, 14679 (1996).

[33] See, for example, the Fermi surface plots by C. Lehmann, S. Sinning, P. Zahn, H. Wonn, and I. Mertig at `http://www.phy.tu-dresden.de/~fermisur/`.

[34] M. D. Stiles and D. R. Penn, Phys. Rev. B **61**, 3200 (2000).